ARTICLES
PUBLISHED ONLINE: 14 DECEMBER 2015 | DOI: 10.1038/NGEO2608
nature geoscience

Links between tropical Pacific seasonal, interannual and orbital variability during the Holocene

J. Emile-Geay[1]*, K. M. Cobb[2], M. Carré[3], P. Braconnot[4], J. Leloup[5], Y. Zhou[1], S. P. Harrison[6], T. Corrège[7], H. V. McGregor[8], M. Collins[9], R. Driscoll[10], M. Elliot[11], B. Schneider[12] and A. Tudhope[10]

The El Niño/Southern Oscillation (ENSO) is the leading mode of interannual climate variability. However, it is unclear how ENSO has responded to external forcing, particularly orbitally induced changes in the amplitude of the seasonal cycle during the Holocene. Here we present a reconstruction of seasonal and interannual surface conditions in the tropical Pacific Ocean from a network of high-resolution coral and mollusc records that span discrete intervals of the Holocene. We identify several intervals of reduced variance in the 2 to 7 yr ENSO band that are not in phase with orbital changes in equatorial insolation, with a notable 64% reduction between 5,000 and 3,000 years ago. We compare the reconstructed ENSO variance and seasonal cycle with that simulated by nine climate models that include orbital forcing, and find that the models do not capture the timing or amplitude of ENSO variability, nor the mid-Holocene increase in seasonality seen in the observations; moreover, a simulated inverse relationship between the amplitude of the seasonal cycle and ENSO-related variance in sea surface temperatures is not found in our reconstructions. We conclude that the tropical Pacific climate is highly variable and subject to millennial scale quiescent periods. These periods harbour no simple link to orbital forcing, and are not adequately simulated by the current generation of models.

ENSO, the oscillatory instability of the tropical Pacific ocean–atmosphere system, is the leading pattern of global interannual variability, with important physical, ecological and human impacts[1]. Yet, predicting its long-term behaviour in the face of continued anthropogenic forcing has proved elusive[2]. Whereas the predictive skill of climate models at interannual timescales can be tested using instrumental observations, such records are too short to evaluate the fidelity of model-simulated tropical Pacific variability on adaptation-relevant timescales. This motivates the use of palaeoclimate observations, which cover a much longer time span and predate the instrumental observations used to develop and tune climate models, hence providing an out-of-sample test of their predictive ability[3].

The mid-Holocene (MH, about 6,500 yr before present; 6.5 kyr BP) represents a key target for evaluating the simulated response of ENSO to external forcing. Whereas ice volume and greenhouse gas concentrations were essentially similar to today, the latitudinal and seasonal distribution of incoming solar radiation (insolation) was markedly different as a result of precession[4]: seasonal contrast was amplified in the Northern Hemisphere and reduced in the Southern Hemisphere. Thus, the MH provides an opportunity to explore the link between changes in the seasonal cycle, meridional asymmetry in the equatorial zone, and ENSO behaviour. Several circum-Pacific palaeoclimate records have been interpreted as implying a marked reduction in ENSO activity during the MH (refs 5–7), a reduction simulated by models of various complexity[8–13]. Furthermore, this reduction has been dynamically linked either to changes in the linear stability of ENSO (ref. 9), or to an insolation-driven increase in the amplitude of the annual cycle in near-equatorial sea surface temperature (SST; hereafter, AC; refs 9,10,12), in line with evidence for a negative correlation between ENSO and the AC documented in instrumental observations[14] and modelling studies of current and past climate states[8,15–19].

Several mechanisms have been proposed to account for the seasonal cycle influence on ENSO: frequency locking[15,20]; nonlinear resonance between annual and internal modes[21,22]; and combination tones of ENSO and the AC (ref. 23). We note, however, that the inverse link between ENSO variance and AC amplitude is not universal amongst models[4,10] nor in the various proposed mechanisms. Whereas some seasonally resolved palaeoclimate records suggest a strong dynamical link between precessional forcing and ENSO activity[24], reconstructions of central and eastern Pacific ENSO variance do not[25,26]. A synthesis of the available observations and simulations of ENSO and the annual cycle is timely, and would help constrain ENSO sensitivity to external forcing.

Here we synthesize high-resolution, well-dated palaeoclimate records from across the tropical Pacific spanning the Holocene

[1]Department of Earth Sciences, University of Southern California, Los Angeles, California 90089, USA. [2]School of Earth and Atmospheric Sciences, Georgia Institute of Technology, Atlanta, Georgia 30332, USA. [3]Institut des Sciences de l'Evolution, Université de Montpellier, CNRS, IRD, EPHE, Montpellier 34095, France. [4]IPSL/LSCE, unité mixte CEA-CNRS-UVSQ, Gif sur Yvette 91191, France. [5]Sorbonne Universités, UPMC Univ. Paris 6, LOCEAN/IPSL, UMR 7159, CNRS-IRD-MNHN, 75005 Paris, France. [6]Centre for Past Climate Change and School of Archaeology, Geography and Environmental Sciences (SAGES), University of Reading, Whiteknights, Reading RG6 6AB, UK. [7]Université Bordeaux, UMR CNRS 5805 EPOC, Allee Geoffroy St Hilaire, 33615 Pessac cedex, France. [8]School of Earth and Environmental Sciences, University of Wollongong, Wollongong, New South Wales 2522, Australia. [9]College of Engineering, Mathematics and Physical Sciences, University of Exeter, Laver Building, North Park Road, Exeter EX4 4QE, UK. [10]University of Edinburgh, School of GeoSciences, James Hutton Road, Edinburgh EH9 3FE, UK. [11]Paleoclimats Paleoenvironnements Bioindicateurs, Université de Nantes, LPGNantes, 2 rue de la Houssinière, Nantes 44300, France. [12]Institut für Geowissenschaften, Universität Kiel, D-24118 Kiel, Germany. *e-mail: julieneg@usc.edu

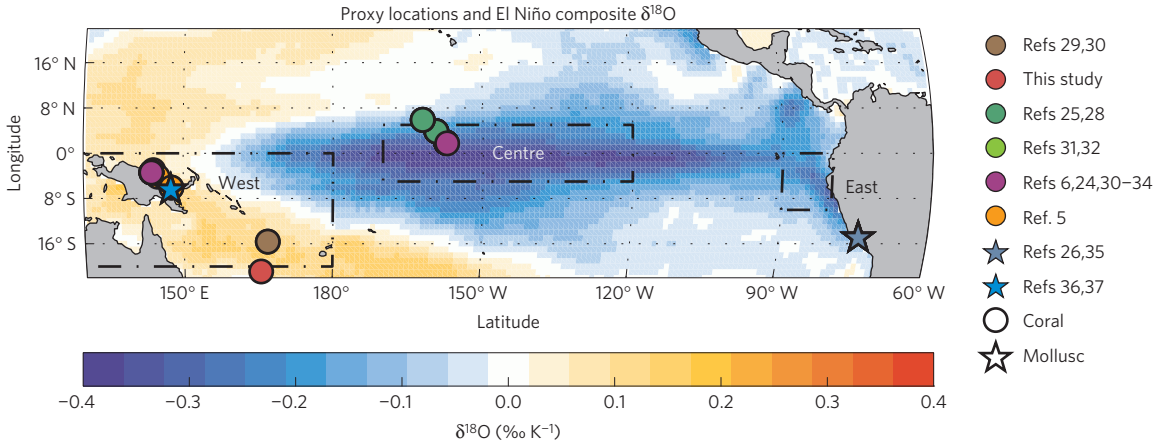

Figure 1 | Location and ENSO sensitivity of proxy archives. Circles denote corals; stars denote molluscs. Contours denote biocarbonate $\delta^{18}O$ composites (‰ per °C of NINO3.4 SST) derived from the model of ref. 39 driven by NCEP OI analysis v2 SST and SODA 2.2.4 SSS over 1981–2010 boreal winters (Supplementary Figs 8 and 9). $\delta^{18}O$ values were regressed onto NINO3.4 SST to highlight relationships to ENSO. The three equatorial study regions (west, centre and east) are delineated by rectangles. Note that refs 11,12,15,16,18–21 all use data from Kiritimati (1° 53′ N, 157° 24′ W).

(see Methods). We compare these observations with an ensemble of nine state-of-the-art global climate models (GCMs) from the Paleoclimate Modelling Intercomparison Project[27] (PMIP3), which include simulations of pre-industrial (PI; piControl) as well as industrial (historical) and MH (midHolocene) climate (Supplementary Table 2). This data set constitutes the most comprehensive collection of oxygen isotope measurements on Holocene corals[5,6,24,25,28–34] and molluscs[26,35–37] so far from the tropical Pacific (Fig. 1 and Supplementary Table 1 and Supplementary Figs 1–6). Such marine carbonates record the isotopic composition of oxygen ($\delta^{18}O$), which reflects changes in SST (Supplementary Fig. 10a) as well as the $\delta^{18}O$ of sea water (the latter linearly related to sea surface salinity (SSS, Supplementary Fig. 10b). The isotopic signal is generally dominated by the thermal component, except in the far western Pacific (Supplementary Fig. 11). All records have annual or finer resolution and collectively cover ~2,000 out of the past 10,000 years (Supplementary Table 1 and Supplementary Fig. 1). There are three clusters of sites in the western (WP, Papua New Guinea, New Caledonia, Vanuatu, Surprise Atoll), central (CP, the Line Islands of Palmyra, Fanning and Christmas) and eastern (EP, Peruvian coast) tropical Pacific.

Seasonal and interannual variability over the Holocene

The seasonal and interannual components of the tropical Pacific records show much irregularity in interannual (2–7 yr) variance—a measure of ENSO activity—as well as in AC amplitude. To enable comparisons between different records and sites, we show the ratio between fossil and modern (twentieth century) values of interannual variance and AC amplitude (Fig. 2), with uncertainties estimated with the block bootstrap (Methods). Most records of ENSO variance plot below unity, implying that twentieth-century ENSO was unusually active[25,38]. Those fossil samples exhibiting higher-than-modern ENSO variance have large uncertainties compatible with no change. Such uncertainties are usually the consequence of short fossil and/or modern sequences.

Despite appreciable differences between ENSO reconstructions from the three regions, some consistent patterns do emerge. In the WP (Fig. 2, top), the records show a significant decrease in ENSO variance during the early and mid-Holocene[5,6,29,36]; there are only a few records from the 6–2 kyr BP interval but these also show reduced ENSO variance. Low ENSO variance is present throughout the past 7 kyr in the CP (Fig. 2, centre), with the most consistent signal corresponding to a 64% reduction occurring between 3–5 kyr BP (Table 1) and a trend from extremely low variance to the present state from 2 kyr BP onwards[24,25]. Records from the EP show ENSO variance either similar to or lower than today, with the deepest reduction around 4.6 kyr BP (Fig. 2, bottom)[26]. Thus, our data set suggests that the MH reduction in ENSO variance identified in previous studies[5–7,32] is not an exceptional event, but rather that ENSO may have been less active than at present for much of the Holocene.

Reconstructions of the AC amplitude exhibit little coherence through time. Records from the WP show AC amplitudes similar to present before 7 kyr BP. However, records from the interval 7–4 kyr BP unequivocally exhibit a reduced AC amplitude, whereas after 3 kyr BP the records show a return to AC amplitudes similar to the present day. In contrast, records from the CP show considerable temporal structure in AC amplitude, although many of the individual records have high levels of uncertainty. In the EP, the records show slightly reduced AC amplitude throughout the past 10 kyr, except for a period with amplitude similar to the present day at 3 kyr BP.

Comparisons with simulated tropical Pacific climates

We now use this data set to constrain the behaviour of PMIP3 models. Although there are comparatively few records from precisely 6.5 kyr BP, we assume that the changes recorded during the window between about 7.5 and 5.5 kyr BP are representative of the MH and provide an indication of the average change to be expected in the MH simulations. To make quantitative model–data comparisons, we translate model output into oxygen isotope ratios using a forward modelling approach[39,40], in which the $\delta^{18}O$ of biocarbonates is parameterized as a function of SSS and SST (Methods). This approximates the isotopic variations that would have been recorded by the coral or mollusc in response to the simulated changes in climate produced by each climate model, which can then be directly compared with the observed variations at a site (Supplementary Figs 10 and 11). The forward model is a simplified representation of the incorporation of ^{18}O by mollusc and coral systems, in particular because it represents the relationship between seawater ^{18}O and SSS as time-invariant. However, it has been shown to reproduce the first-order basin-scale variability contained in modern corals from across the tropical Pacific[39]. Thus, this simple model provides a way of bridging GCMs and palaeo observations.

Most of our records are comparatively short: the average record length is around 50 years (Supplementary Fig. 1b) and very few are longer than 100 years. As ENSO variability is non-stationary,

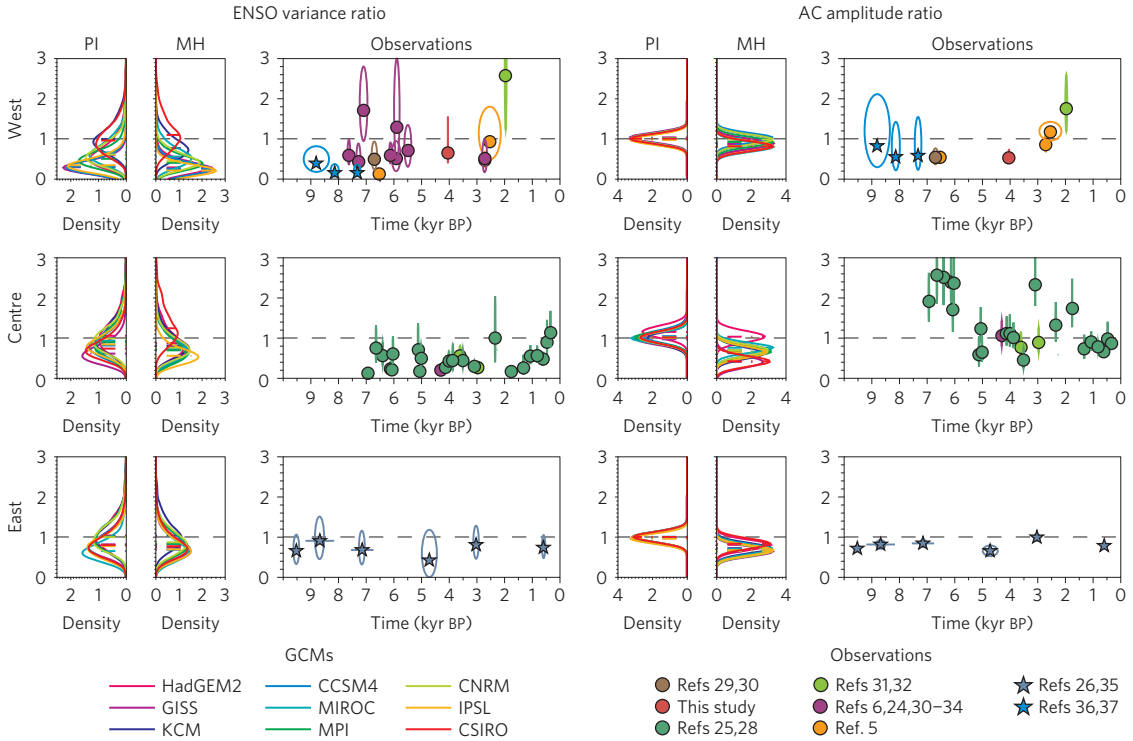

Figure 2 | Distribution of seasonal and interannual variability in models and observations. Top: changes in ENSO variance and AC amplitude over the Holocene. Left column: changes in ENSO-band (2–7 yr) variance between fossil and modern samples in the west (top), centre (middle) and east (bottom). Horizontals bars mark the period covered by each data set; except for molluscs from the Peruvian coast, these are narrower than the symbol width. Ellipses represent uncertainties about these ratios in both dimensions: the width represents a 95% CI for the central date of each sample, based on reported analytical uncertainty on radiometric ages; the vertical component is a 95% CI for the variance ratio, obtained through a block-bootstrap procedure (Methods). Unity (no change) is marked by a dashed grey line. Similar statistics derived from PMIP3 models on 50-yr windows are depicted on side panels for piControl and midHolocene experiments. Solid lines are kernel density estimates of those distributions (Methods), whereas dashed lines indicate their median. Right column: *idem* for AC amplitude.

quantifying ENSO variance over such short windows leads to a wide range of estimates[41,42]. Random sampling of multi-century model simulations under stationary boundary conditions shows that ENSO variance estimates on 50-year windows may vary by up to ±50% from sampling alone (Supplementary Fig. 13); these estimates converge as the observation window lengthens. Thus, the short length of most of the observations could make it difficult to discriminate between observed and simulated variability. Changes in the AC amplitude are much better constrained, although still sensitive to segment length (Supplementary Figs 12 and 13).

For each model, we estimate the statistical distributions of modelled ENSO and AC amplitude for 50-year periods using the block bootstrap for both the piControl and midHolocene simulations (Supplementary Table 2) and compare these distributions to the values obtained from the historical simulations (Supplementary Figs 14–22). The distributions of ENSO variance ratios are broad and positively skewed, whereas those of AC amplitude are narrow and symmetric (Fig. 2, coloured curves). ENSO variance ratios are clustered around unity in the piControl experiments, and fall below unity in most of the midHolocene experiments. The midHolocene reduction is small and, given the width of the distributions, only marginally significant at the 5% level. Nonetheless, it is qualitatively consistent with results from an intermediate complexity model[8] as well as many other GCM simulations[9–13], all of which show reduced ENSO variability during the MH compared with the PI climate.

Although the synthesis of existing palaeo-ENSO data presents a heterogeneous picture of ENSO variability through both space and time, there is evidence for a sustained reduction in ENSO variability from 3–5 kyr BP. This is especially true in the CP, where a deep reduction (64%) is accompanied by a relatively narrow 95% confidence interval (CI) of [28%, 84%] (Table 1). Reductions of similar magnitude are observed during the MH (5.5–7.5 kyr BP; 66% in the centre, 50% in the west, 33% in the east), albeit with CIs so wide that they cannot exclude increases in ENSO variance (Table 1). Thus, a salient feature of this data set is a robust, approximately two-thirds reduction in CP interannual variance, which seems to have persisted throughout much of the 3–5 kyr BP interval. This persistent reduction bears little resemblance to the model simulations of reduced MH ENSO (refs 4,8) followed by a gradual intensification to the present[13], and happened at a time when boreal summer/winter precessional forcing was weaker than during the MH (Supplementary Fig. 9).

Table 1 | Observed reductions in ENSO variance in the tropical Pacific during the MH (5.5–7.5 kyr BP) and the 3–5 kyr BP interval.

		Quantiles		
Period	**Region**	**2.5%**	**50%**	**97.5%**
5.5–7.5 kyr BP	West	−125%	50%	92%
	Centre	−5%	66%	92%
	East	−16%	33%	69%
3–5 kyr BP	West	−54%	35%	61%
	Centre	28%	64%	84%
	East	−18%	58%	109%

The numbers represent quantiles of the block-bootstrap ensembles. By convention, a negative reduction implies an increase.

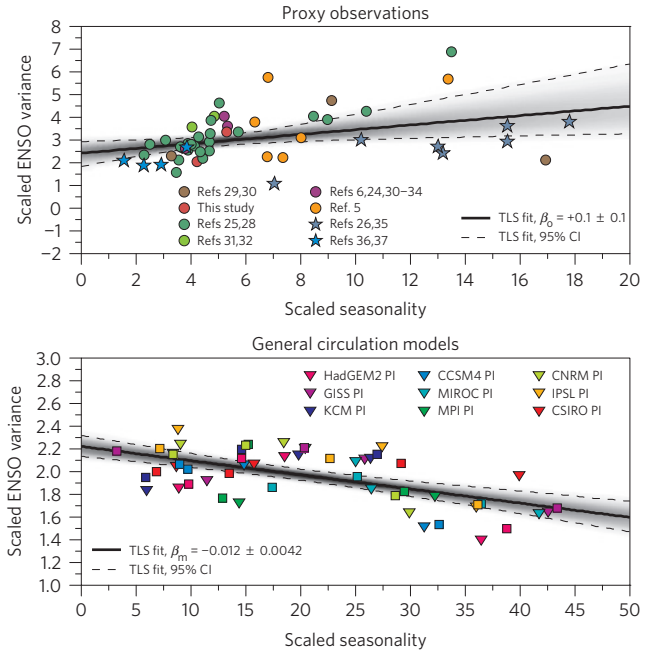

Figure 3 | Link between interannual and seasonal variability in models and observations. Link between ENSO variance and the seasonal cycle in proxy observations (top) and PMIP3 models (bottom). The observed values are for all seasonally resolved records from the Pacific during the whole of the past 10 kyr. The simulated values are based on 50-year segments from the midHolocene and piControl simulations. On top, symbology as in Fig. 1. On the bottom, triangles denote the median of piControl simulations, squares the median of midHolocene simulations. Data from the EP, CP and WP were pooled together, scaled by their interquartile range so their uncertainties on both axes are commensurate. An orthogonal regression (total least squares, TLS) fit is presented for both data sets, together with approximate 95% CIs (dashed lines) and probability density (grey contours) obtained through bootstrap resampling (Methods).

Can PMIP3 GCMs simulate the magnitude of such reductions, and if so, under which conditions? We answer this question by computing the probability of observing ENSO variance reductions of at least 64% on 50-year segments (Table 2). These probabilities are extremely low under PI conditions, ranging from 1 to 12%. Such occurrences are still rare under MH boundary conditions (probabilities ranging from 3 to 15%), although most (7 out of 9) of the models show an increased probability of ENSO reduction. Thus, whereas orbital forcing characteristic of the MH tends to drive simulated changes in ENSO variance in the right direction, the amplitude of simulated changes is too modest, and the response is not consistent among models. It is even harder to explain the larger, more sustained reductions that may have prevailed during the 3–5 kyr BP period, but the short length of the simulations (Supplementary Table 2) precludes an assessment of this question.

The models all show a reduction in the median amplitude of the AC in the midHolocene simulations, for all three regions. The reduction is between 10 and 50% (depending on the model) but is relatively uniform across the basin (Fig. 2, right). This uniformity contrasts strongly with the observed changes in the 7.5–5.5 kyr BP window, where AC amplitude is decreased in the WP but increased in the CP. However, the reduction in AC amplitude in the WP is ~50% larger than in the simulations.

Links between ENSO and the seasonal cycle amplitude

We investigate the link between changes in ENSO variance and in AC amplitude by plotting the fossil to modern ratio of ENSO-band variance against the same ratio of AC amplitude, in both Holocene observations and PMIP3 simulations (Fig. 3). Both axes are scaled by their uncertainty to make an orthogonal regression possible (Methods). The simulated relationship is significantly negative (Fig. 3, bottom), in agreement with previous work[17–20]. This contrasts with the observations, which reveal a weak positive relationship between ENSO variance and AC amplitude (Fig. 3, top). Moreover, the range of variations in AC amplitude is about 2–3 times larger in the observations than in the simulations (Supplementary Fig. 23). Similar results emerge if only data from the CP are considered (Supplementary Figs 24 and 25), or if wavelet analysis is used to diagnose the relationship between energy in the annual and interannual bands[19] (Methods and Supplementary Fig. 26). If our interpretation of the data is correct, the mismatch between the observed and simulated relationship between ENSO variance and AC amplitude has important dynamical implications. The frequency entrainment hypothesis[15,20] states that a self-exciting oscillator will give up its independent mode of oscillation and acquire the frequency of the applied forcing (in this case, the AC in insolation). It has long been invoked to explain the inverse relationship between ENSO and the AC in coupled GCMs (refs 12,13,17,18). Our results confirm that this link is strong in PMIP3 models, but suggest that it is opposite to that found in observations over the Holocene.

In comparing the ENSO–AC relationship across models and data, it is important to note the limitations associated with using a sparse set of observations to constrain tropical Pacific dynamics. One possible explanation for the model–data mismatch in the ENSO–AC relationship is that uncertainties in AC amplitude estimates from corals are more uncertain than depicted by the bootstrap intervals, as documented by discrepancies of up to 30% in AC estimates from overlapping coral $\delta^{18}O$ records from the CP (Supplementary Fig. 12). The relationship between $\delta^{18}O$ and SSS is poorly constrained on subannual scales, and may vary across a given reef environment, further confounding estimates of AC amplitude changes from high-resolution archives. Results are, however, insensitive to the choice of ENSO metric as long as fossil/modern ratios are used (Supplementary Fig. 27).

Changes in the spatial characteristics of ENSO represent another source of uncertainty, as different flavours of ENSO have different impacts on SST and SSS across the study domain. Canonical El Niño events involve temperature changes in the EP. However, many events peak in the CP (ref. 43). Indeed, changes in the prevalence of ENSO flavours in the Holocene have been suggested by changes in the asymmetry of ENSO anomalies in the EP (ref. 26) as well as analysis of PMIP3 midHolocene simulations[12,44]. Thus, some of the observed variations in ENSO intensity/frequency over the Holocene could reflect changes in the spatial pattern of ENSO and differences between individual records could reflect a dominance of one expression of ENSO over another[26]. However, an empirical

Table 2 | Probability of observing periods of reduced ENSO activity in the CP in nine GCMs.

H_0	HadGEM2	GISS	KCM	CCSM4	MIROC	MPI	CNRM	IPSL	CSIRO
PI null	1.37%	11.98%	1.62%	3.66%	2.82%	3.55%	0.88%	2.06%	5.00%
MH null	3.12%	3.16%	3.35%	5.60%	7.36%	9.78%	3.81%	15.50%	0.21%

Top row: frequency of occurrence of 50-year-long periods for which the ENSO variance ratio is as low as the 3–5 kyr BP average inferred from palaeoclimate observations (0.36—a 64% reduction) in pre-industrial (piControl) simulations. Bottom row: same for midHolocene simulations.

ENSO model suggests that modern changes in the prevalence of ENSO flavours may arise internally[45]. Our data set is too sparse to resolve spatial features of ENSO or the AC structure, but it is hoped that denser proxy networks will shed light on these questions in the future.

Implications for ENSO dynamics

It has been suggested that boreal autumn insolation, which peaks at ~5 kyr BP (Supplementary Fig. 8), modulates ENSO variability through air/sea coupling strength[8]. Our analyses reveal that changes in ENSO variance and AC amplitude over the Holocene bear no simple relation to orbital forcing, excluding a linear mechanism. It is possible that millennial-scale changes in ENSO variability arose: internally; or as a nonlinear response to orbital forcing; or because of other factors, such as the presence of a remnant Laurentide ice sheet, which modulated the response to orbital forcing[46]. Our observations suggest persistent changes in ENSO variance and AC amplitude that fall well outside the range shown by both piControl and midHolocene PMIP3 simulations, particularly during the 3–5 kyr BP interval. The PMIP3 ensemble does not capture the potential range of ENSO variability over this interval, which should become a key target for climate models of varying complexity to simulate and explain. One challenge in simulating such changes with GCMs is that computational requirements restrict simulations to 200–500 yr, on average. Additional long transient runs, both forced[13] and unforced[41], would help distinguish endogenous from exogenous sources of ENSO variability. Furthermore, the simulated relationship between ENSO variance and AC amplitude is incompatible with observations. GCMs where an inverse relationship to AC amplitude dominates the ENSO response to orbital forcing may therefore not be representative of the real world. Given that the mean state, AC and ENSO are so tightly connected[16,47], the substantial climatological biases in the fifth phase of the Coupled Modelling Intercomparison Project (CMIP5) models[48] are a logical suspect for this exaggerated relationship. Of particular relevance is the SST–shortwave feedback[49], the asymmetric nature of which is not captured by many state-of-the-art GCMs (ref. 48). Even those GCMs that qualitatively simulate the feedback may do so through error compensation, so we speculate that large improvements in ENSO simulations would result from a correct representation of the underlying processes.

Whereas precessional and greenhouse gas forcing are fundamentally different in character, our work demonstrates the ability of high-resolution palaeoclimate records to provide fundamental constraints on tropical climate dynamics, as represented in models used to project twenty-first-century climate trends. In that context, the fact that ENSO seemed relatively impervious to a large external forcing suggests that processes internal to the climate system could dominate external influences. Understanding internal processes of low-frequency ENSO modulation, and the extent to which they are captured by climate models, is therefore of utmost importance to improving climate projections.

Methods

Methods and any associated references are available in the online version of the paper.

Received 9 April 2015; accepted 29 October 2015; published online 14 December 2015

References

1. Sarachik, E. S. & Cane, M. A. *The El Niño-Southern Oscillation Phenomenon* 336–384 (Cambridge Univ. Press, 2010).
2. Collins, M. *et al.* The impact of global warming on the tropical Pacific Ocean and El Niño. *Nature Geosci.* **3,** 391–397 (2010).
3. Schmidt, G. A. Enhancing the relevance of palaeoclimate model/data comparisons for assessments of future climate change. *J. Quat. Sci.* **25,** 79–87 (2010).
4. Braconnot, P., Luan, Y., Brewer, S. & Zheng, W. Impact of Earth's orbit and freshwater fluxes on Holocene climate mean seasonal cycle and ENSO characteristics. *Clim. Dynam.* **38,** 1081–1092 (2012).
5. Tudhope, A. W. *et al.* Variability in the El Niño-Southern Oscillation through a glacial-interglacial cycle. *Science* **291,** 1511–1517 (2001).
6. McGregor, H. V. & Gagan, M. K. Western Pacific coral $\delta^{18}O$ records of anomalous Holocene variability in the El Niño-Southern Oscillation. *Geophys. Res. Lett.* **31,** L11204 (2004).
7. Koutavas, A. & Joanides, S. El Niño-Southern Oscillation extrema in the Holocene and Last Glacial Maximum. *Paleoceanography* **27,** PA4208 (2012).
8. Clement, A. C., Seager, R. & Cane, M. A. Suppression of El Niño during the mid-Holocene by changes in the Earth's orbit. *Paleoceanography* **15,** 731–737 (2000).
9. Liu, Z., Kutzbach, J. & Wu, L. Modeling climate shift of El Niño variability in the Holocene. *Geophys. Res. Lett.* **27,** 2265–2268 (2000).
10. Zheng, W., Braconnot, P., Guilyardi, E., Merkel, U. & Yu, Y. ENSO at 6 ka and 21 ka from ocean–atmosphere coupled model simulations. *Clim. Dynam.* **30,** 745–762 (2008).
11. Chiang, J. C. H., Fang, Y. & Chang, P. Pacific climate change and ENSO activity in the mid-Holocene. *J. Clim.* **22,** 923–939 (2009).
12. An, S.-I. & Choi, J. Mid-Holocene tropical Pacific climate state, annual cycle, and ENSO in PMIP2 and PMIP3. *Clim. Dynam.* **43,** 957–970 (2014).
13. Liu, Z. *et al.* Evolution and forcing mechanisms of El Niño over the past 21,000 years. *Nature* **515,** 550–553 (2014).
14. Wang, X. L. The coupling of the annual cycle and ENSO over the tropical Pacific. *J. Atmos. Sci.* **51,** 1115–1136 (1994).
15. Chang, P., Wang, B., Li, T. & Ji, L. Interactions between the seasonal cycle and the Southern Oscillation—frequency entrainment and chaos in a coupled ocean-atmosphere model. *Geophys. Res. Lett.* **21,** 2817–2820 (1994).
16. Guilyardi, E. El Niño mean state seasonal cycle interactions in a multi-model ensemble. *Clim. Dynam.* **26,** 329–348 (2006).
17. Timmermann, A., Lorenz, S. J., An, S.-I., Clement, A. & Xie, S.-P. The effect of orbital forcing on the mean climate and variability of the tropical Pacific. *J. Clim.* **20,** 4147–4159 (2007).
18. An, S.-I. *et al.* The inverse effect of annual-mean state and annual-cycle changes on ENSO. *J. Clim.* **23,** 1095–1110 (2010).
19. An, S.-I. & Choi, J. Inverse relationship between the equatorial eastern Pacific annual-cycle and ENSO amplitudes in a coupled general circulation model. *Clim. Dynam.* **40,** 663–675 (2013).
20. Liu, Z. A simple model study of ENSO suppression by external periodic forcing. *J. Clim.* **15,** 1088–1098 (2002).
21. Tziperman, E., Stone, L., Cane, M. A. & Jarosh, H. El Niño chaos: overlapping of resonances between the seasonal cycle and the Pacific ocean-atmosphere oscillator. *Science* **264,** 72–74 (1994).
22. Jin, F.-F., Neelin, J. D. & Ghil, M. El Niño on the Devil's staircase: annual subharmonic steps to chaos. *Science* **264,** 70–72 (1994).
23. Stuecker, M. F., Timmermann, A., Jin, F.-F., McGregor, S. & Ren, H.-L. A combination mode of the annual cycle and the El Niño-Southern Oscillation. *Nature Geosci.* **6,** 540–544 (2013).
24. McGregor, H. V. *et al.* A weak El Niño-Southern Oscillation with delayed seasonal growth around 4,300 years ago. *Nature Geosci.* **6,** 949–953 (2013).
25. Cobb, K. M. *et al.* Highly variable El Niño-Southern Oscillation throughout the Holocene. *Science* **339,** 67–70 (2013).
26. Carré, M. *et al.* Holocene history of ENSO variance and asymmetry in the eastern tropical Pacific. *Science* **345,** 1045–1048 (2014).
27. Braconnot, P. *et al.* Evaluation of climate models using palaeoclimatic data. *Nature Clim. Change* **2,** 417–424 (2012).
28. Cobb, K. M., Charles, C. D., Cheng, H. & Edwards, R. L. El Niño/Southern Oscillation and tropical Pacific climate during the last millennium. *Nature* **424,** 271–276 (2003).
29. Duprey, N. *et al.* Early mid-Holocene SST variability and surface-ocean water balance in the southwest Pacific. *Paleoceanography* **27,** PA4207 (2012).
30. Kilbourne, K. H., Quinn, T. M., Taylor, F. W., Delcroix, T. & Gouriou, Y. El Niño-Southern Oscillation-related salinity variations recorded in the skeletal geochemistry of a *Porites* coral from Espiritu Santo, Vanuatu. *Paleoceanography* **19,** PA4002 (2004).
31. Woodroffe, C. D. & Gagan, M. K. Coral microatolls from the central Pacific record Late Holocene El Niño. *Geophys. Res. Lett.* **27,** 1511–1514 (2000).
32. Woodroffe, C. D., Beech, M. R. & Gagan, M. K. Mid-late Holocene El Niño variability in the equatorial Pacific from coral microatolls. *Geophys. Res. Lett.* **30,** 1358 (2003).
33. Evans, M., Fairbanks, R. & Rubenstone, J. A proxy index of ENSO teleconnections. *Nature* **394,** 732–733 (1998).

34. McGregor, H. V., Fischer, M. J., Gagan, M. K., Fink, D. & Woodroffe, C. D. Environmental control of the oxygen isotope composition of *Porites* coral microatolls. *Geochim. Cosmochim. Acta* **75,** 3930–3944 (2011).
35. Carré, M., Sachs, J. P., Schauer, A. J., Rodríguez, W. E. & Ramos, F. C. Reconstructing El Niño-Southern Oscillation activity and ocean temperature seasonality from short-lived marine mollusk shells from Peru. *Palaeogeogr. Palaeoclimatol. Palaeoecol.* **371,** 45–53 (2013).
36. Driscoll, R. *et al.* ENSO reconstructions over the past 60 ka using giant clams (*Tridacna* sp.) from Papua New Guinea. *Geophys. Res. Lett.* **41,** 6819–6825 (2014).
37. Welsh, K., Elliot, M., Tudhope, A., Ayling, B. & Chappell, J. Giant bivalves (*Tridacna gigas*) as recorders of ENSO variability. *Earth Planet. Sci. Lett.* **307,** 266–270 (2011).
38. McGregor, S., Timmermann, A., England, M. H., Elison Timm, O. & Wittenberg, A. T. Inferred changes in El Niño-Southern Oscillation variance over the past six centuries. *Clim. Past* **9,** 2269–2284 (2013).
39. Thompson, D. M., Ault, T. R., Evans, M. N., Cole, J. E. & Emile-Geay, J. Comparison of observed and simulated tropical climate trends using a forward model of coral $\delta^{18}O$. *Geophys. Res. Lett.* **38,** L14706 (2011).
40. Dee, S. G. *et al.* PRYSM: an open-source framework for proxy system modeling, with applications to oxygen-isotope systems. *J. Adv. Mod. Earth Syst.* **7,** 1220–1247 (2015).
41. Wittenberg, A. T. Are historical records sufficient to constrain ENSO simulations? *Geophys. Res. Lett.* **36,** L12702 (2009).
42. Russon, T., Tudhope, A. W., Hegerl, G. C., Schurer, A. & Collins, M. Assessing the significance of changes in ENSO amplitude using variance metrics. *J. Clim.* **27,** 4911–4922 (2014).
43. Kug, J.-S., Jin, F.-F. & An, S.-I. Two types of El Niño events: cold tongue El Niño and warm pool El Niño. *J. Clim.* **22,** 1499–1515 (2009).
44. Karamperidou, C., Di Nezio, P. N., Timmermann, A., Jin, F.-F. & Cobb, K. M. The response of ENSO flavors to mid-Holocene climate: implications for proxy interpretation. *Paleoceanography* **30,** 527–547 (2015).
45. Newman, M., Shin, S.-I. & Alexander, M. A. Natural variation in ENSO flavors. *Geophys. Res. Lett.* **38,** L14705 (2011).
46. Luan, Y., Braconnot, P., Yu, Y. & Zheng, W. Tropical Pacific mean state and ENSO changes: sensitivity to freshwater flux and remnant ice sheets at 9.5 ka BP. *Clim. Dynam.* **44,** 661–678 (2015).
47. Roberts, W. H. G., Battisti, D. S. & Tudhope, A. W. ENSO in the mid-Holocene according to CSM and HadCM3. *J. Clim.* **27,** 1223–1242 (2013).
48. Bellenger, H., Guilyardi, E., Leloup, J., Lengaigne, M. & Vialard, J. ENSO representation in climate models: from CMIP3 to CMIP5. *Clim. Dynam.* **42,** 1999–2018 (2014).
49. Lloyd, J., Guilyardi, E. & Weller, H. The role of atmosphere feedbacks during ENSO in the CMIP3 models. Part III: the shortwave flux feedback. *J. Clim.* **25,** 4275–4293 (2012).

Acknowledgements

We acknowledge the World Climate Research Program's Working Group on Coupled Modelling, which is responsible for CMIP, and we thank the PMIP3 modelling groups for producing and making available their model output. The US Department of Energy's Program for Climate Model Diagnosis and Intercomparison provides coordinating support for CMIP, and led development of software infrastructure in partnership with the Global Organization for Earth System Science Portals. J.E.-G. acknowledges support from US NSF grant DMS 1025465. K.M.C. acknowledges support from NOAA award NA11OAR4310166 and NSF award OCE-0752091. M.Collins acknowledges support from UK NERC grant NE/H009957/1. H.V.M. and A.T. acknowledge support from Australian Research Council (ARC) Discovery Project grant DP1092945. H.V.M. is supported by an ARC Future Fellowship FT140100286 grant. A.T. acknowledges support from UK NERC grant NE/H009957/1. T.C. thanks M. McCulloch (formerly at ANU) for dating the Bayes coral, and M. Gagan's team at ANU for help with isotopic measurements. The Bayes 1 core was collected with funds from the Institut de Recherche pour le Développement. B.S. was supported by the DFG Cluster of Excellence 'The Future Ocean' (EXC 80/2). P.B., M.Carré, T.C., J.L., M.E. and A.T. were supported by the French National Research Agency under EL PASO grant (no. 2010 298 BLANC 608 01). This project also serves for coordination and implementation of the PMIP3/CMIP5 simulations on the ESGF distributed database. We thank J.-Y. Peterschmitt for his help with the PMIP database. This work was initiated in a workshop co-sponsored by WCRP/CLIVAR, IGBP/PAGES, INQUA and IPSL in 2011.

Author contributions

J.E.G. designed the study, performed the analysis, led the writing, and prepared the manuscript. P.B. coordinated the synthesis. M.Carré, K.M.C., T.C., M.E. and R.D. contributed data and/or analysis. P.B. and J.L. analysed simulations and contributed to writing. Y.Z. processed PMIP3 output and generated some of the supplementary figures. A.T., B.S. and M.Collins provided input in the analysis and interpretation. J.E.G., K.M.C., M.Carré, S.P.H., H.V.M., T.C., P.B. and A.T. wrote the paper. All authors reviewed the manuscript.

Additional information

Supplementary information is available in the online version of the paper. Reprints and permissions information is available online at www.nature.com/reprints. Correspondence and requests for materials should be addressed to J.E.-G.

Competing financial interests

The authors declare no competing financial interests.

Methods

Observational synthesis. We compiled oxygen isotopic records ($\delta^{18}O$) obtained from coral or mollusc aragonitic skeletons from 65 sites in the Pacific (Supplementary Table 1). Most of the records have been published[5,6,24–26,28–37], but some are published for the first time here (Supplementary Information). Most of the individual records are comparatively short (50 years or less, Supplementary Fig. 1). The records sample 2,162 years out of the past 10,000 years (Supplementary Fig. 1 and Supplementary Table 1).

For analytical purposes, we group the individual sites into three separate regions: west [120°, 180°, 20° S, 0°], including Papua New Guinea and New Caledonia; centre [170° W, 120° W, 5° S, 5° N], corresponding to the NINO3.4 region (for which the SST average is a key ENSO indicator) and encompassing part of the Line Islands; east [90° W, 80° W, 5° S, 5° N], corresponding to the NINO1+2 regions, a primary region to monitor coastal warming.

Figure 1 shows that these three climatically meaningful regions encompass most of the sites. Note that the sites of ref. 26, although formally outside the NINO1+2 region (eastern box), are interpreted as recording NINO1+2 SST (ref. 35).

Analysis of observations. Changes in ENSO variance were quantified by computing the ratio of fossil to modern variance in the 2–7 yr band. In continuous records, the latter was isolated by means of a (Morlet) wavelet filter (Supplementary Fig. 7), whereas for Peruvian molluscs we used the ratio of fossil to modern variance of the distribution of the annual cycle $\delta^{18}O$ amplitude[35], a proxy for interannual variance in NINO1+2 SST. Results are not sensitive to the filter type or exact metric (Supplementary Information). AC amplitude was quantified as the range (maximum minus minimum) of a monthly mean seasonal cycle evaluated over each record's time span after high-pass filtering the data with a 10-year smoothing spline[50,51] to avoid the biasing effect of trends. Changes in this quantity were, likewise, computed as a ratio between fossil and modern samples.

Uncertainties in ENSO variance and AC amplitude ratios were estimated using a block-bootstrap procedure[52,53] with 1,000 draws. For interannual variance, the block length was set at 2 years, and for seasonal amplitude the block length was set to the number of samples per year. Both choices reflect a compromise between the approximate decorrelation time of the records and the shortness of some proxy records. For Peruvian molluscs, uncertainties were estimated through Monte Carlo simulations as described in ref. 54. The procedure is similar to a block-bootstrap analysis with 5,000 draws and block lengths of 1 year using an instrumental time series sampled and disturbed by simulated proxy-related noise sources.

Climate models and simulations. We consider the simulations that have been run as part of the fifth phase of the Coupled Modelling Intercomparison Project[55] (CMIP5) and analysed in the third phase of the Palaeoclimate Modelling Intercomparison Project[27] (PMIP3). This set of simulations is usually referred to as the CMIP5/PMIP3 experiments, although here we simply refer to them as PMIP3 experiments. The models used (Supplementary Table 2) are state-of-the-art coupled ocean–atmosphere general circulation models (GCMs), or Earth system models with different levels of complexity in the forcing used or in the interactions between climate and the carbon cycle[56]. We consider three experimental designs, following PMIP3 nomenclature.

piControl: the reference is pre-industrial simulations for which Earth's orbit and solar constant are representative of modern conditions. Trace gases concentrations, land use and aerosol loadings are prescribed to their AD 1850 values. The prescribed values vary slightly from one model to the other. Details are given in https://wiki.lsce.ipsl.fr/pmip3/doku.php/pmip3:design:pi:final.

midHolocene: for the mid-Holocene we use simulations in which Earth's orbital parameters and trace gases have been prescribed to those valid for 6 kyr BP (ref. 27). In all of the simulations the date of the vernal equinox is fixed to 21 March at noon. The insolation forcing at the Equator is shown in Supplementary Fig. 9 (see also ref. 57 and Fig. 3). Details are given in https://wiki.lsce.ipsl.fr/pmip3/doku.php/pmip3:design:6k:final.

Historical: to test the impact of the reference period on the analyses of the simulated change in the different climates we also consider historical simulations[55] forced with time evolution of trace gases, volcanic forcing and land use over the period 1860–2005. We sampled from the full ensemble of HIST simulations, including several runs with slightly different initial conditions for each model. In general, their ENSO statistics were indistinguishable from PI within uncertainties.

Forward modelling of marine bicarbonates. Although $\delta^{18}O$ in marine biocarbonates predominantly reflects either SST (refs 58–60) or seawater $\delta^{18}O$ variations resulting from net surface freshwater balance[61,62], most corals and molluscs are affected by both variables. This problem may be directly addressed by explicitly modelling the relationship between the environmental variables and the observed $\delta^{18}O$ (that is, forward modelling[40,63]). Unlike empirical calibration, forward models do not require assumptions to be made about linearity, the independence of predictors, or the normality of residuals.

A reasonably complete model of the incorporation of ^{18}O in coral aragonite requires information on local ocean temperature, seawater ^{18}O, pH, insolation and nutrients. However, ref. 39 developed a simple bivariate model to predict the ^{18}O of coral aragonite using SST and SSS as sole inputs. SSS acts as a proxy for seawater ^{18}O, with regionally dependent coefficients calibrated over the instrumental era. The thermal dependence is set at $-0.22‰\,°C^{-1}$, close to the expected slope for inorganic equilibrium fractionation[64]. This model has been shown to capture first-order variations in the hydrologic response of coral oxygen isotopic composition[39,65]. There are known limitations to the use of such a simple model[65–67]. Specifically, it ignores coral biology and non-equilibrium effects, which are thought to explain some low-frequency trends in corals[68]. Further, the SSS–$^{18}O_{sw}$ slope may not be constant on millennial timescales[69], and its spatial variations may severely bias the estimation of palaeo-ENSO variability, particularly in the WP (ref. 65). Nevertheless, we use this model to translate climate model outputs into a ^{18}O signal for comparison with the observations because very few of the climate models explicitly simulate water isotopes. The same model may be applied to simulate $\delta^{18}O$ values in the shells of *Tridacna* sp. and *Mesodesma donacium*[26,36,37] because they precipitate aragonite like corals. The slope of the SST–$\delta^{18}O$ relationship generally used for aragonitic molluscs ranges from -0.21 to $-0.27‰\,°C^{-1}$ (refs 70,71), compatible with the slope of $-0.22‰\,°C^{-1}$ used by ref. 39.

We note that recent studies have attempted to quantify uncertainties in inferring changes in ENSO variance from calibrated proxy observations[42,72]. By using a process model, we eschew some of the difficulties associated with calibration, but this passes the uncertainties on to the process model. Additionally, ref. 72 neglected sampling uncertainties, which are central to our analysis. The existence of non-climatic noise is a problem in every palaeoclimate data set, and the reader is referred to the original studies for an appraisal of the strength of each climate signal.

Analysis of GCM simulations. GCM-simulated SST and SSS were translated to $\delta^{18}O$ values using the forward model described above. The ensuing 'pseudocoral' fields were averaged over the three main regions (WP, CP, EP), and then resampled using the above-mentioned block-bootstrap procedure with $N = 1{,}000$ draws, before being subsampled on contiguous 50-year blocks to emulate short observational windows (Supplementary Information and Supplementary Figs 13–22). We then computed ENSO variance and AC amplitude, as well as their ratios, for each ensemble member. Probability distributions from these 1,000 member ensembles were then obtained using kernel density estimation with a bandwidth $h = 0.15$ (Fig. 2).

Regression analysis. We used total least-squares (TLS) regression (a form of error-in-variables modelling, closely connected to orthogonal regression[73]), to account for uncertainties in the ENSO–AC amplitude relationship. TLS steepens regression slopes by taking the potentially biasing effects of observational noise into account[74]. ENSO variance and AC amplitude ratios were scaled by their uncertainty (measured by the interquartile range of their block-bootstrap distributions) before TLS regression, to ensure homogeneous error magnitudes on both axes of Fig. 3. Uncertainties in regression parameters are estimated through a bootstrap approach[75], with 2,000 draws.

Wavelet analysis. The relationship between ENSO and the AC is also probed through Morlet wavelet analysis[76]. As in ref. 19, we sum the energies corresponding to the 2–7 yr and 0.8–1.2 yr bands and report linear correlations between the resulting series. We do so for all seasonally resolved, continuous records in the database (that is, all except those of refs 26,35) and for the PMIP3 piControl and midHolocene model outputs, separately for each of the three geographic regions. Statistical significance is established by means of a non-parametric, isospectral test[77], which accounts for the loss of degrees of freedom imparted by smoothing by low-frequency wavelets.

Data. Data for the palaeo observations and model output for the three areas outlined in Fig. 1 are available at https://github.com/CommonClimate/EmileGeay_NatGeo2015. The original model data were obtained via the CMIP5/PMIP3 portal (http://cmip-pcmdi.llnl.gov/cmip5), and the published palaeo data were obtained from the National Climatic Data Center (https://www.ncdc.noaa.gov/data-access/paleoclimatology-data).

Code availability. The code to reproduce all of the figures and tables in this manuscript is publicly available. Specifically, Matlab/Python code to reproduce the block-bootstrap, wavelet and regression analysis is available at https://github.com/CommonClimate/EmileGeay_NatGeo2015. These codes generate the probability distributions for all of the ratios plotted in Fig. 2, except those associated with ref. 26. The Matlab code to generate the latter distributions is available at http://www.isem.univ-montp2.fr/carre_matthieu, using the parameter

values published in ref. 54 (SOM). See the ReadMe.md file at https://github.com/CommonClimate/EmileGeay_NatGeo2015 for more detailed instructions.

References

50. Cook, E. R. & Peters, K. The smoothing spline: a new approach to standardizing forest interior tree-ring width series for dendroclimatic studies. *Tree-Ring Bull.* **41,** 45–53 (1981).
51. Weinert, H. L. A fast compact algorithm for cubic spline smoothing. *Comput. Stat. Data Anal.* **53,** 932–940 (2009).
52. Efron, B. & Tibshirani, R. J. *An Introduction to the Bootstrap* (Chapman & Hall, 1993).
53. Kunsch, H. R. The jackknife and the bootstrap for general stationary observations. *Ann. Stat.* **17,** 1217–1241 (1989).
54. Carré, M., Sachs, J. P., Wallace, J. M. & Favier, C. Exploring errors in paleoclimate proxy reconstructions using Monte Carlo simulations: paleotemperature from mollusk and coral geochemistry. *Clim. Past* **8,** 433–450 (2012).
55. Taylor, K. E., Stouffer, R. J. & Meehl, G. A. An overview of CMIP5 and the experiment design. *Bull. Am. Meteorol. Soc.* **93,** 485–498 (2011).
56. Flato, G. *et al.* in *Climate Change 2013: The Physical Science Basis* (eds Stocker, T. F. *et al.*) 741–866 (IPCC, Cambridge Univ. Press, 2013).
57. Luan, Y., Braconnot, P., Yu, Y., Zheng, W. & Marti, O. Early and mid-Holocene climate in the tropical Pacific: seasonal cycle and interannual variability induced by insolation changes. *Clim. Past* **8,** 1093–1108 (2012).
58. Dunbar, R. B., Wellington, G. M., Colgan, M. W. & Glynn, P. W. Eastern Pacific sea surface temperature since 1600 A.D.: the $\delta^{18}O$ record or climate variability in Galápagos corals. *Paleoceanography* **9,** 291–316 (1994).
59. Evans, M., Fairbanks, R. & Rubenstone, J. The thermal oceanographic signal of El Niño reconstructed from a Kiritimati Island coral. *J. Geophys. Res.* **104,** 13409–13422 (1999).
60. Cobb, K. M., Charles, C. D. & Hunter, D. E. A central tropical Pacific coral demonstrates Pacific, Indian, and Atlantic decadal climate connections. *Geophys. Res. Lett.* **28,** 2209–2212 (2001).
61. Fairbanks, R. G. *et al.* Evaluating climate indices and their geochemical proxies measured in corals. *Coral Reefs* **16,** S93–S100 (1997).
62. Conroy, J. L., Cobb, K. M., Lynch-Stieglitz, J. & Polissar, P. J. Constraints on the salinity–oxygen isotope relationship in the central tropical Pacific Ocean. *Mar. Chem.* **161,** 26–33 (2014).
63. Evans, M. N., Tolwinski-Ward, S. E., Thompson, D. M. & Anchukaitis, K. J. Applications of proxy system modeling in high resolution paleoclimatology. *Quat. Sci. Rev.* **76,** 16–28 (2013).
64. McConnaughey, T. ^{13}C and ^{18}O isotopic disequilibrium in biological carbonates: I. Patterns. *Geochim. Cosmochim. Acta* **53,** 151–162 (1989).
65. Russon, T., Tudhope, A. W., Hegerl, G. C., Collins, M. & Tindall, J. Inter-annual tropical Pacific climate variability in an isotope-enabled CGCM: implications for interpreting coral stable oxygen isotope records of ENSO. *Clim. Past* **9,** 1543–1557 (2013).
66. Stevenson, S., McGregor, H. V., Phipps, S. J. & Fox-Kemper, B. Quantifying errors in coral-based ENSO estimates: toward improved forward modeling of $\delta^{18}O$. *Paleoceanography* **28,** 633–649 (2013).
67. Thompson, D. M. *et al.* Coral-model comparison highlighting the role of salinity in long-term trends. *PAGES Newsl.* **21,** 60–61 (2013).
68. Lough, J. A strategy to improve the contribution of coral data to high-resolution paleoclimatology. *Palaeogeogr. Palaeoclimatol. Palaeoecol.* **204,** 115–143 (2004).
69. LeGrande, A. N. & Schmidt, G. A. Water isotopologues as a quantitative paleosalinity proxy. *Paleoceanography* **26,** PA3225 (2011).
70. Grossman, E. L. & Ku, T.-L. Oxygen and carbon isotope fractionation in biogenic aragonite: temperature effects. *Chem. Geol.* **59,** 59–74 (1986).
71. Carré, M. *et al.* Stable isotopes and sclerochronology of the bivalve *Mesodesma donacium*: potential application to Peruvian paleoceanographic reconstructions. *Palaeogeogr. Palaeoclimatol. Palaeoecol.* **228,** 4–25 (2005).
72. Russon, T., Tudhope, A. W., Collins, M. & Hegerl, G. C. Inferring changes in ENSO amplitude from the variance of proxy records. *Geophys. Res. Lett.* **42,** 1197–1204 (2015).
73. Van Huffel, S. *Total Least Squares and Errors-in-Variables Modeling: Bridging the Gap between Statistics, Computational Mathematics and Engineering* 539–555 (Physica-Verlag, 2004).
74. Markovsky, I., Sima, D. M. & Van Huffel, S. Total least squares methods. *Wiley Interdiscip. Rev.* **2,** 212–217 (2010).
75. Pešta, M. Total least squares and bootstrapping with applications in calibration. *Statistics* **47,** 966–991 (2013).
76. Torrence, C. & Compo, G. P. A practical guide to wavelet analysis. *Bull. Am. Meteorol. Soc.* **79,** 61–78 (1998).
77. Ebisuzaki, W. A method to estimate the statistical significance of a correlation when the data are serially correlated. *J. Clim.* **10,** 2147–2153 (1997).